Number spectra of nonequilibrium neutrinos from neutron stars: Impact of realistic nuclear interactions and free hyperons

A. Dehghan Niri and H. R. Moshfegh
Department of Physics, University of Tehran, P.O. Box 14395-547, Tehran, Iran

(Received 29 August 2021; revised 24 February 2022; accepted 11 March 2022; published 28 April 2022)

The number spectrum of nonequilibrium neutrinos resulting from neutron star matter deviation from beta equilibrium is calculated. For this purpose, the chemical potential gap ($\delta\mu$) in a typical density change and in the high degeneracy regime ($k_BT \leqslant 0.1$ MeV) is estimated. This is done under the application of realistic descriptions of nuclear matter and the assumption of the presence of free hyperons (Σ^-, Λ^0) in the neutron star core. Realistic nuclear interactions are taken into account by a microscopic many-body approach—the lowest order constrained variational (LOCV) method—for asymmetric nuclear matter. We find that addition of a three-body force interaction leads to a dramatic change in the trend of the symmetry energy at high densities and consequently the change in the sign of $\delta\mu$. This, as a result, changes the dominant flavor of the nonequilibrium neutrinos. By accounting for the hyperons' presence, we see that apart from the sign change of $\delta\mu$ its value can change noticeably. In hypernuclear matter, the effect of particle fractions is also very important. We have also investigated the effect of deviation from beta equilibrium on the dynamic part of the number spectra of nonequilibrium neutrinos produced in the neutron branch of the modified Urca process. It is shown that this part of the number spectra is not affected significantly by the nonequilibrium process and can be replaced by its equilibrium value.

DOI: 10.1103/PhysRevC.105.045809

I. INTRODUCTION

Physics of neutron stars (NSs) is a suitable substrate for the interplay between the equation of state (EoS) of dense matter and the properties of these densest objects in the observable universe. Among these properties is the cooling rate of NSs and neutrino emission from their interiors is the dominating cooling mechanism before the internal temperature falls to 10^8 K [1]. The emissivity of neutrinos is calculated by assuming equilibrium with respect to weak interactions. In fact, since equilibrium with respect to other interactions, i.e., strong and electromagnetic ones, is achieved very fast, weak interactions are the only interactions that determine the final full thermodynamic beta equilibrium state of the star. However, in the NS case, the term *full* deserves a comment: NS medium in temperatures less than 10^9 K is highly degenerate and as a result, transparent to neutrinos [2]. So, under this condition, neutrinos freely escape from the interior of a NS and there is no concentration of them in the star. This makes neutrino emission processes irreversible and attaining full thermodynamic equilibrium impossible. But fortunately, due to the high degeneracy of the core constituents of a NS, the available phase space (that, in the condition of final equilibrium, is determined by the finite value of the temperature) is small. Therefore the energy carried away by neutrinos compared to the Fermi energy of other species is small, too. Hence, application of the term *full* is almost justified.

In a simple model of a NS core made up of a large number of neutrons (n), with an admixture of protons (p) and electrons (e), for fulfilling electrical neutrality and obtaining the beta equilibrium, the composition of matter is characterized by the proton fraction among the total number of baryons (nucleons in npe matter), $Y_p = \frac{n_p}{n_b}$ (where n_p is the number density of protons and n_b is the number density of baryons). Y_p depends on the local density. It is determined by the minimization of the total energy of the system, including the rest masses under the constraint of baryon number conservation and charge neutrality, while adopting a specific many-body method and a strong interaction model. This, as a whole, is equivalent to the charge current weak interactions $n \to p + e^- + \overline{\nu}_e$ and $p + e^- \to n + \nu_e$ (traditionally called by the exotic name *Urca* in the context of stellar evolution [3]) running with the same rates. In view of working in a high degeneracy regime, such a condition means $\mu_n = \mu_p + \mu_e$, where μ_i is the chemical potential of the ith specie. Hereafter, we refer to this latter equality as the *chemical potential balance relation*. This also implies the equality of ν_e and $\overline{\nu}_e$ emissivities.

Muons can be present in the medium. Their presence is allowed when the electrons' Fermi energy ($E_{F(e)}$) (or, in a high degeneracy condition, their chemical potential) exceeds the rest energy of the muons, i.e., $E_{F(e)} = c(m_e^2c^2 + p_{F(e)}^2)^{1/2} \simeq p_{F(e)}c > m_\mu c^2 = 105.56$ MeV, where $p_{F(e)}$ is the electron Fermi momentum. Since under high degeneracy condition and neglecting thermal corrections Fermi momenta are $p_{F_i} = (3\pi^2 n_i)^{1/3}\hbar$, the muons' number density is obtained by their chemical potential balance with electrons ($\mu_e = \mu_\mu$). This is a result of a local equilibrium with respect to relevant weak interactions $e^- \to \mu + \nu_e + \overline{\nu}_\mu$, $\mu \to e^- + \overline{\nu}_e + \nu_\mu$. This condition along with the Urca process then establishes the full thermodynamic beta equilibrium in $npe\mu$ matter. Clearly, the beta equilibrium among n, p, and μ is the same as that among n, p, and e. We put our focus on the one with electrons.

When the density in the NS medium increases it is economical, from the energy point of view, that massive baryons (more probably hyperons) appear in the system instead of an increase in the number density of the lighter baryons [4]. Each hyperon is produced in a reaction that satisfies energy and momentum conservation simultaneously and its number density is obtained through chemical potential balance in that reaction. This chemical potential balance relation along with the one related to the muon production and finally that related to the nucleon Urca process form the full thermodynamic beta equilibrium in $npe\mu Y$ matter (Y refers to hyperons). Notice that hyperons, when they appear, undergo their own Urca process, e.g., $\Sigma^- \rightarrow \Lambda^0 + e^- + \nu_e^-$ and $\Lambda^0 + e^- \rightarrow \Sigma^- + \nu_e$. These interactions can possibly compete with the nucleon Urca process in neutrino production and even dominate over it. However, focusing on the nucleon Urca process is adequate for the purpose of our study.

Depending on the proton concentration at each instant toward final equilibrium (Y_p), two types of Urca process, direct (dUrca) and modified (mUrca), can occur and lead to neutrino production: dUrca is the Urca process allowed by simultaneous energy and momentum conservation laws. MUrca, on the other hand, occurs when the mentioned conservation condition is not satisfied and Urca has to proceed with the contribution of an additional particle that provides the energy and momentum mismatch (sSee Ref. [3] for a detailed description). Clearly, the additional particle does not participate in the chemical potential balance relation.

It is possible to consider various external or macroscopic phenomena that change the density of the NS matter. If this change of the density of the matter elements occurs on a timescale (τ_ρ) much longer than the beta equilibration timescale (τ_β), the assumption of beta equilibrium remains valid (adiabatic density change). However, since the matter is strongly degenerate in the NS core the available phase space for beta reactions, responsible for constructing the new equilibrium state, is limited due to the Pauli exclusion principle. Hence, τ_β is expected to be much longer than τ_ρ (see Appendix A that checks validity of this expectation in our work). In view of this condition, there can be relevant astronomical scenarios that lead to a departure from the beta equilibrium state which have their own observational footprints. Radial pulsations of the NSs lead to local compression and rarefaction of matter with $\approx$ millisecond periods, which are much shorter than the β reaction timescale at $k_B T \leqslant 0.1$ MeV (k_B is the Boltzman constant). So, they induce deviation from chemical potential balance. Neutrino emission from the nonequilibrium mUrca process was studied in several contexts as the damping mechanism for the small amplitude radial pulsations of the NS, slowing down its cooling [5–8]. NS vibrations can be a source of a large amount of energy by changing the thermodynamic equilibrium state. The energy stored in the vibrations can be released through various phenomena. In a paper by Langer and Cameron, the electromagnetic observability of vibrating NSs was explored [9]. It was indicated that reaction rates for hyperon weak interactions can damp the vibrations rapidly enough to make the electromagnetic observability of these stars probable. NSs with their mass near the maximum allowable value, determined by general relativity and an assumed nuclear EoS, can possibly have a fate of collapsing into a black hole if their mass increases through an accretion process. The rapid monotonic compression of NS matter (on the timescale of a fraction of millisecond [10]) in the precollapse stage leads to the departure from beta equilibrium, and a short burst of neutrinos is expected to accompany the collapse. The upper bounds for this neutrino burst was estimated in a paper by Gourgoulhon and Haensel [10] using the parametrized EoS of asymmetric nuclear matter of Prakash *et al.* [11]. The contraction of the NS matter due to its spin-down leads to the change of chemical potential state. Reisenegger investigated the reduction of the net cooling rate due to the conversion of some amounts of the stored chemical energy into thermal energy and even the possibility of a net heating, and the effect of this heating mechanism on the thermal evolution of NSs [12].

In all of the above phenomena, the departure from chemical equilibrium, measured and characterized by the chemical potential gap value and sign, $\delta\mu = \mu_n - \mu_p - \mu_e$, is the determining factor. As was already mentioned, particle fractions are determined by beta equilibrium reactions (Urca) along with those weak interactions responsible for the appearance of other species (μ, Σ^-, Λ^0 in our work). As a result, the Urca process (direct or modified) is characteristic of the final equilibrium state. When a rapid change of the local density occurs, the concentration of the matter constituents, due to the slowness of the weak interaction rates, is no longer in an equilibrium state. Depending on the assumed EoS for describing the NS core and the corresponding symmetry energy behavior, the system becomes protonized or neutronized compared with the new equilibrium state in each specified baryon density. Therefore, a nonequilibrium state characterized by the chemical potential gap $\delta\mu$ arises. This breaking of chemical equilibrium ($\delta\mu \neq 0$) opens an additional volume in the phase space through which the Urca process can proceed with different rates (depending on $\delta\mu$ sign, one more intensively than the other) and bring the matter to a new beta equilibrium state (Le Châtelier's principle). The other species' (μ, Σ^-, Λ^0) equilibration reactions guarantee their appearance and determine their concentrations at each instant (characterized by proton fraction) towards the new full thermodynamic beta equilibrium state. As a consequence, in the rapid change of the density (compared with beta reaction rates) of NS matter, from any origin, $\delta\mu$ and its sign are the key ingredients. They are directly related to the assumed density-dependant features of matter above nuclear saturation density and so can offer another opportunity for diagnosing superdense matter properties. The purpose of this paper is to investigate the importance of applying realistic descriptions of the NS medium and the presence of new degrees of freedom (free hyperons) on the value of $\delta\mu$ (chemical potential gap) and its sign and applying the results in determining the number spectra of nonequilibrium neutrinos. $\delta\mu$ is a function of time but we restrict our exploration to the initial moment [$\delta\mu(n_b, Y_p, t = 0)$] of a small compression (such that $\delta\mu \ll \mu_i$, which guarantees the strong degeneracy related to the opened nonthermal phase space). As a typical example, we consider the change in the density happening for $n_b = 0.9\ \mathrm{fm}^{-3}$ and increasing it to $1.0\ \mathrm{fm}^{-3}$. For those instances in which dUrca is inactive and so mUrca is responsible for the new beta equilibrium state, we explore the effect of such a sudden compression on the dynamic part of the mUrca process too. We pursue our goal by applying a microscopic many-body method with realistic two-body interactions as the input. We also study the effect of the three-body force and the presence of free hyperons (Σ^-, Λ^0) on our results. The microscopic many-body method employed in our work is a modified extended version of the lowest order constrained variational (LOCV) method: a fully self-consistent variational method that has been successful in describing various properties of baryonic systems in the last three decades [13–16]. The applied realistic two-body interactions are Argonne V18 (AV18) [17] and Reid 68 [18] potentials. The three-body interaction employed is a phenomenological Urbana type potential (UIX). Notice that accounting for the hyperon-nucleon and hyperon-hyperon interactions can influence $\delta\mu$ through changing nucleon and electron chemical potentials, but we limit our calculations to the case of free hyperons. It is a reasonable assumption because it is good enough for attaining some insight into the $\delta\mu$ value sensitivity to the appearance of new species and for presenting a schematic view of the importance of this effect while avoiding the complexity arising from accounting for the hyperon interactions. Furthermore, in the LOCV method, $\Lambda\Lambda$ and Λ-nucleon interactions are the only interactions currently accounted for [19]. So, assuming the hyperons to be free in the adopted many-body scheme and in our $npe\mu\Sigma^-\Lambda^0$ model of the NS core again seems to give more general outcomes.

The paper proceeds as follows. The number spectrum of nonequilibrium electron neutrinos in dUrca and mUrca processes is calculated briefly in Sec. II. In Sec. III, the dependence of $\delta\mu$ on nuclear symmetry energy in the absence and presence of free hyperons is explained. Section IV is devoted to the obtained results. Our discussions and conclusions are presented in Sec. V. To justify that within our realistic descriptions of the NS core the beta equilibration timescale is actually long enough compared with the density changing timescale, we present an estimation of the beta relaxation time in Appendix A. A brief review of the modified extended version of the LOCV approach is also outlined in Appendix B.

II. NUMBER SPECTRA OF NONEQUILIBRIUM NEUTRINOS

Consider the simplest model of a NS core made up of n, p, e, and probably μ. Assume that n and p form a "normal" Fermi liquid (i.e., $T > T_c$, where T_c is the temperature below which superfluidity for neutrons and superconductivity for protons is expected). The electrons and muons are considered as a normal noninteracting Fermi gas. Each of these constituents is separately in thermodynamic equilibrium, with chemical potentials μ_i ($i = n, p, e, \mu$), and strongly degenerate ($\mu_i \gg k_B T$). The effects of the presence of other particles (free hyperons) are discussed later. Weak interactions (Urca process), neutron beta decay ($n \to p$)

$$n \to p + e^- + \overline{\nu}_e \tag{1}$$

and electron capture ($p \to n$)

$$p + e^- \to n + \nu_e, \tag{2}$$

proceeding with the same rates guarantee the beta equilibrium state. This means $\Gamma_{n\to p} = \Gamma_{p\to n}$, where Γ is the neutrino number emissivity, i.e., the number of neutrinos emitted from $1\ \mathrm{cm}^3$ during one second. As mentioned before, if the simultaneous energy and momentum conservation is satisfied, neutrinos are produced via dUrca; otherwise, an active spectator is needed to provide the energy and momentum difference and the neutrino production proceeds through mUrca. From a practical viewpoint, this means that there is a threshold density below which only mUrca reactions can occur while for densities above that value only the dUrca process plays the key role. Furthermore, the presence of the active spectator in mUrca affects the rate of neutrino production through occupying some domains of the available phase space of (1) and (2), and it complicates the calculation of the production rate by direct presence in the interaction Hamiltonian density operator (see Ref. [20] and the references therein).

Let us suppose that the assumed NS undergoes an astronomical process that results in a rapid change of the local density. The number spectrum of non-equilibrium neutrinos, which is dominantly nonthermal, is given by $\frac{d\Gamma}{dy}$ where $y = \frac{E_\nu}{k_B T}$ and E_ν is the neutrino energy. Several studies have been dedicated to the nonequilibrium beta processes in the NS core [12,21]. In this section, by focusing on the nonequilibrium neutrinos' number spectra, we give a brief summary of the previously obtained results. We shall start with the simpler neutrino production mechanism, that is dUrca.

A. Direct Urca process

The dUrca reaction requires the condition $p_{F_n} < p_{F_p} + p_{F_e}$ to be satisfied. In an npe model of the NS core, this corresponds to $p_{F_n} < 2p_{F_p}$ or $Y_p^{(\text{dUrca-}npe)} > {}^1/_9$ (obviously, muon presence shifts this threshold to higher values). Reaching this threshold depends on the EoS and mainly on the behavior of the symmetry energy. It is typically satisfied at several times the nuclear saturation density, $n_0 = 0.16\ \mathrm{fm}^{-3}$. Let us suppose that the required condition is obtained.

In a nonequilibrium condition, the number of antineutrinos with their momentum near $\vec{p}_{\overline{\nu}}$ (or their energy between $E_{\overline{\nu}}$ and $E_{\overline{\nu}} + dE_{\overline{\nu}}$), produced in a unit volume and in one second, is different from that of neutrinos with the same energy, and is given by

$$d\Gamma_{n\to p} = \frac{d^3 p_{\overline{\nu}}}{(2\pi\hbar)^3} \mathcal{W}_{n\to p}(E_{\overline{\nu}}) \tag{3}$$

where, for reaction (1),

$$\begin{aligned}\mathcal{W}^{(d)}_{n\to p}(E_{\overline{\nu}}) = \int &\frac{d^3 p_n}{(2\pi\hbar)^3} \frac{d^3 p_p}{(2\pi\hbar)^3} \frac{d^3 p_e}{(2\pi\hbar)^3} f_n(E_n)[1 - f_p(E_p)] \\ &\times [1 - f_e(E_e)](2\pi)^4 \delta(E_n - E_p - E_e - E_{\overline{\nu}}) \\ &\times \delta^3(\vec{p}_n - \vec{p}_p - \vec{p}_e - \vec{p}_{\overline{\nu}}) \langle |\mathcal{M}^{(d)}_{n\to p}|^2 \rangle. \end{aligned} \tag{4}$$

Here, $\langle|\mathcal{M}^{(d)}_{n\to p}|^2\rangle$ is the squared transition amplitude in dUrca (hence the index d) averaged over initial spin states and summed over the final spins, and $f_i(E_i) = \{1+\exp[(E_i-\mu_i)/k_BT]\}^{-1}$ is the Fermi-Dirac distribution function for the fermion specie with the energy E_i. For reaction (2), $f_n[1-f_p][1-f_e]$ in (4) is replaced with $[1-f_n]f_pf_e$. δ functions enclose the required condition for the total energy and momentum conservation. Owing to the strong degeneracy condition ($k_BT \leqslant 0.1$ MeV and $\delta\mu \ll \mu_i$), the method of the theory of Fermi liquids is applicable [22]. This consists of setting $p = p_F$ in all smooth energy and momentum functions under the integral, leading to the decoupling of the integration over particle momenta from those over the energies. This is the so-called phase space decomposition that greatly simplifies the above integrations [23]. For n, p, and e, $d^3p_i \cong p_{F_i}m_i^*dE_id\Omega_i$, where m_i^* is the effective mass of the ith specie and $d\Omega_i$ is the solid angle in the direction of $\vec{p}_i$. For neutrinos, $d^3p_\nu \cong E_\nu^2/c^3dE_\nu d\Omega_\nu$. Angular integrations are then performed analytically. We shall not go through the details of the whole calculation; it can be found in Ref. [23].

Using the previously introduced variable $y = \frac{E_\nu}{k_BT}$ and defining the dimensionless variables $x_i = \frac{E_i-\mu_i}{k_BT}$, where $i = n, p, e$ and $\xi = \frac{\delta\mu}{k_BT}$, the integration over particle energies in (4) becomes

$$I^{(d)}_{n\to p}(y-\xi) = (k_BT)^2\int_{-\infty}^{+\infty} dx_ndx_pdx_e \times\delta(x_n-x_p-x_e-(y-\xi)) \times f(x_n)[1-f(x_p)][1-f(x_e)]. \tag{5}$$

Doing the above integration is straightforward by applying the symmetry property $1-f(x) = f(-x)$. We finally arrive at

$$\frac{d\Gamma^{(d)}_{n\to p}(y-\xi)}{dy} = \frac{G^2\left(1+3c_A^2\right)m_n^*m_p^*m_e^*}{8\pi^5\hbar^{10}c^3}(k_BT)^2 \times y^2\mathcal{F}_d(y-\xi) \tag{6}$$

where the function $\mathcal{F}_d$ is defined by

$$\mathcal{F}_d(y) \equiv \frac{y^2+\pi^2}{e^y+1}. \tag{7}$$

G and c_A are the Fermi weak coupling constant and the axial vector renormalization, respectively. Replacing the effective mass of the ultrarelativistic electrons with $m_e^* \cong p_{F_e}/c$ and substituting the numerical values of the constants, we obtain the following formulas for the number spectra of the nonequilibrium antineutrinos produced in (1):

$$\frac{d\Gamma^{(d)}_{n\to p}}{dy} = 8.75\times10^{31}\left(\frac{n_b}{n_0}\right)^{1/3}Y_e^{1/3}\frac{m_n^*m_p^*}{m_n^2}T_9^5 \times y^2\mathcal{F}_d(y-\xi)\ [\mathrm{cm^{-3}s^{-1}}], \tag{8}$$

where m_n is the neutron bare mass and $T_9 = T/10^9$ K. The number spectrum of the neutrinos produced in (2) follows a similar relation except that the argument of $\mathcal{F}_d$ is replaced with $y+\xi$.

B. Modified Urca process

If the dUrca threshold is not satisfied, active participation of an additional particle (a nucleon in $npe\mu$ matter) in (1) and (2) can lead to the required energy and momentum balance in strongly degenerate NS matter. In this case, we have to deal with the mUrca process, modified neutron beta decay ($n\to p$)

$$n+N\to N+p+e^-+\overline{\nu}_e \tag{9}$$

and modified electron capture ($p\to n$)

$$p+N+e^-\to N+n+\nu_e, \tag{10}$$

where $N = n$ or p. Because of the low abundance of protons in the medium, the proton branch (p branch) of mUrca has a threshold, too. We limit our calculations to the neutron branch (n branch) which is more efficient [3].

The calculation of the nonequilibrium neutrino production rate in mUrca is similar to that of dUrca, except that the participation of the extra particle in mUrca complicates the calculation of the transition amplitude. In fact, because of the lack of knowledge of the strong interaction between nucleons in high density matter, the treatment of the nucleon-nucleon (N-N) interaction in initial and final states of (9) and (10) is only approximately possible. In a previous work [20], we applied an independent-pair approximation for nucleon quasiparticles [24,25] and used realistic N-N correlation functions for calculating mUrca transition amplitude and neutrino emissivity in beta equilibrium condition. In the present work, we apply the same expression for the transition amplitude of the n branch of mUrca as in Ref. [20]. Starting from relation (3) and following the same path as in dUrca, we arrive at the following statement for the number spectra of antineutrinos produced in (9):

$$\frac{d\Gamma^{(m)}_{n\to p}}{dy} = 5\times10^{21}\frac{Y_p^{1/3}Y_e^{2/3}}{Y_n^2}\frac{n_0}{n_b}\left(\frac{m_n^*}{m_n}\right)^3\left(\frac{m_p^*}{m_p}\right) \times\mathcal{R}(k_{F_n})T_9^7\,y^2\mathcal{F}_m(y-\xi)\ [\mathrm{cm^{-3}s^{-1}}], \tag{11}$$

where the dimensionless factor $\mathcal{R}(k_{F_n})$ (referred to as the correlation factor), with $k_{F_n} = p_{F_n}/\hbar$, is fully introduced in Ref. [20]. It contains the N-N many-body correlation properties through nuclear central and tensor correlation functions. Also,

$$\mathcal{F}_m(y) \equiv \frac{9\pi^4+10\pi^2y^2+y^4}{1+e^y}. \tag{12}$$

The number spectrum of neutrinos from (10) obeys the same formulas as (11) except that the argument of $\mathcal{F}_m$ is replaced with $y+\xi$.

Due to the deviation from beta equilibrium, as was explained before, Y_p in relation (11) refers to the nonequilibrium asymmetry in the new density and all the other particle fractions, the correlation factor and the nucleon effective masses should, in principle, be calculated in the new density in the asymmetry characterized by this Y_p.

III. CHEMICAL POTENTIAL GAP VALUE

A. *npeμ* model

In an $npe\mu$ model of a NS core as asymmetric nuclear matter, the nuclear binding energy per nucleon ($\frac{E_{NN}}{A_N}$) can be expanded in the isospin asymmetry parameter $X = 1 - 2Y_p$. Many-body calculations show that the dependence of E_{NN} on X is, to a very good approximation, quadratic (see, e.g., Refs. [26,27]):

$$\frac{E_{NN}}{A_N}(n_N, X) \simeq \frac{E_0}{A_N}(n_N) + E_{\rm sym}(n_N)X^2, \tag{13}$$

where $\frac{E_0}{A_N} = \frac{E_{NN}}{A_N}(n_N, X = 0)$ is the binding energy per nucleon in symmetric nuclear matter, $n_N = n_n + n_p$ is the nucleon number density, and $E_{\rm sym} \equiv E_{NN}(n_N, X = 1) - E_{NN}(n_N, X = 0)$ is the nuclear symmetry energy. The simple form of (13) enables us to construct an explicit relation between the chemical potential gap value and the density dependence of the symmetry energy in $npe\mu$ matter. Starting from relations $\mu_n = \frac{\partial\varepsilon_{NN}}{\partial n_n}$ and $\mu_p = \frac{\partial\varepsilon_{NN}}{\partial n_p}$, where ε_{NN} is the energy density of bound nucleons, and using the conservation of nucleon number density, we arrive at

$$\mu_n - \mu_p = -\frac{\partial(E_{NN}/A_N)}{\partial Y_p}\bigg|_{n_b} = 4(1 - 2Y_p)E_{\rm sym}. \tag{14}$$

So, in a nonequilibrium condition, for electron neutrino and antineutrino producing processes, we get

$$\delta\mu(n_N, Y_p) = 4(1 - 2Y_p)E_{\rm sym}(n_N) - c\left(m_e^2c^2 + p_{F_e}^2\right)^{1/2}, \tag{15}$$

where the second term in (15) is the electron chemical potential in the free Fermi gas model. The electron fraction, as referred to in the Introduction, is obtained by using the charge neutrality relation ($n_p = n_e + n_\mu$) and its chemical potential balance relation with muons ($\mu_e = \mu_\mu$).

B. Presence of free hyperons

While an $npe\mu$ model is adequate for describing NS matter in densities less than $2n_0$, in densities higher than this value the appearance of other degrees of freedom, more probably from the strange baryon family, i.e., hyperons, is expected [4]. The notable point is that these dense layers of a NS can also be created due to rapid change of density. So, a layer with density in which some specific species (e.g., n, p, e, and μ) can be present only becomes so dense that new particles are allowed to appear. This, as presented in the Results section, can impose a great effect on the value of $\delta\mu$. The stiffness of the EoS plays an important role here: the more stiff an EoS, the more probable is the appearance of new species in lower densities, and so their noticeable effects appear in a wider range of baryon density.

Hyperons, more specifically Σ^- and Λ^0, appear in NS medium when their presence is energetically unavoidable. They can be created in various strangeness violating weak interactions and strangeness conserving strong interactions. For a review of these interactions and how to select the appropriate ones in NS conditions, the reader can refer to Ref. [9]. In the strongly degenerate NS core, the following weak interactions can satisfy the simultaneous energy and momentum conservation and are slow enough to play a role in the nonequilibrium condition:

$$n + n \to p + \Sigma^-, \tag{16}$$

$$n + n \to n + \Lambda^0. \tag{17}$$

In the independent particle model, Σ^-, despite its larger rest mass, appears before Λ^0 because of its negative charge. In fact, it contributes in both baryon number (nucleon plus hyperon numbers) conservation and charge neutrality relations and so its creation is more efficient from the ground state energy point of view. However, in the $npe\mu\Sigma^-\Lambda^0$ model in our work, when the change of the density happens, it is seen that Σ^- abundance exceeds that of the protons in the out-of-equilibrium proton fraction in the new density. We have overcome this problem by allowing Λ^0 to appear first.

Due to (16) and (17), Σ^- and Λ^0 thresholds and abundances in NSs are determined by the following chemical potential balance relations in each baryon density and fixed Y_p and of course by respecting the charge neutrality objective:

$$\mu_{\Sigma^-} = 2\mu_n - \mu_p, \tag{18}$$

$$\mu_\Lambda = \mu_n, \tag{19}$$

where in the free hyperon model μ_{Σ^-} and μ_Λ are calculated within the free Fermi gas model.

Here, we need to obtain the explicit relations of nucleons' chemical potentials in order to apply them in the chemical potential balance relations (18) and (19). These relations are also applied for direct calculation of $\delta\mu$ value. Notice that relation (15) is still valid in the case of the presence of free hyperons, but its application is not justified. That is due to the fact that for its application the constituents' abundances in the nucleonic subsystem are needed, and these data are themselves determined by finding hyperon fractions through using explicit relations of nucleons' chemical potentials.

The starting point for obtaining the nucleons' chemical potentials is again the relation $\mu_i = \frac{\partial\varepsilon_{BB}}{\partial n_i}$ for $i = n, p$ in which ε_{BB} is the total energy density of bound baryons and is related to the total binding energy per baryon as

$$\frac{E_{BB}}{A_B} = \frac{\varepsilon_{BB}}{n_N + n_Y}, \tag{20}$$

where $n_Y = n_{\Sigma^-} + n_{\Lambda^0}$. Since we have assumed the hyperons to be forming a noninteracting free Fermi gas, the contribution from the hyperon-nucleon and hyperon-hyperon interactions is neglected in the above relation. So, for the nucleonic subsystem with binding energy E_{NN} and number density obeying $n_N = n_b - n_{\Sigma^-} - n_{\Lambda^0}$ we can write for each Y_p

$$\mu_i = \frac{\partial\varepsilon_{NN}}{\partial n_i} = \frac{\partial}{\partial n_i}\left(n_N\frac{E_{NN}(n_N, Y_p')}{A_N}\right), \tag{21}$$

exactly the same as a system without hyperons. Again $i = n, p$ and $Y_p' = \frac{n_p}{n_N}$ is the proton fraction within the nucleonic subsystem. By performing a chain derivative in (21) we finally obtain the following relations for the nucleons' chemical potentials:

$$\mu_n(n_N, Y_p') = \left(1 + n_N \frac{\partial}{\partial n_N} - Y_p' \frac{\partial}{\partial Y_p'}\right) \frac{E_{NN}}{A_N}, \tag{22}$$

$$\mu_p(n_N, Y_p') = \left(1 + n_N \frac{\partial}{\partial n_N} + (1 - Y_p') \frac{\partial}{\partial Y_p'}\right) \frac{E_{NN}}{A_N}. \tag{23}$$

The above relations obviously state that the effect of the presence of free hyperons on the nucleons' chemical potentials is only expressed through their contribution in the baryon number.

IV. RESULTS

The main input in relations (8) and (11), which arises from the deviation from beta equilibrium, is the so-called chemical potential gap. Other possibly effective parameters are particle fractions and the correlation factor in the case of the mUrca process. The nucleon effective masses also include the nuclear description properties and can have their own effect on the final result. To investigate the effect of realistic nuclear interactions in the superdense medium of a NS core on the number spectra and flavor of nonequilibrium neutrinos resulting from a typical density change, we have adopted a microscopic many-body framework with realistic two and three-body forces (hereafter 2BFs and 3BFs respectively) as input for strong interactions. The applied many-body approach is the so-called LOCV (a brief description presented in Appendix B) and the realistic 2BF inputs are AV18 and Reid 68. It is well known that the saturation properties of nuclear matter cannot be reproduced by 2BFs only, and adding 3BFs is required to retain consistency with the expected results, especially the existence of $2M_{\odot}$ pulsars. So, we have employed the Urbana IX (UIX) model for 3BFs in a modified extended version of the LOCV method [16] in the case of the AV18 potential to examine the effect of 3BFs on $\delta\mu$ and compare the results with those obtained using 2BFs only. Hereafter, by UIX we mean applying the UIX 3BF model in the manner worked out in Ref. [16].

A. Chemical potential gap

1. npeμ matter

If the baryonic components of the NS matter are supposed to be only n and p, relation (15) is used for estimating $\delta\mu$. The important input in (15), manifesting the specific features of the applied many-body procedure and the nuclear interactions, is E_{sym}. In Fig. 1 we have presented E_{sym} as a function of baryon density, resulting from our realistic descriptions of NS matter in a density range from 0.05 to 1.0 fm^{-3}. The dotted curve shows the symmetry energy when only AV18 2BF is used. As seen, it shows a purely ascending behavior and predicts $E_{\mathrm{sym}}(n_0) = 24.7$ MeV. By adding UIX 3BF effects through applying the modified extended version of LOCV, the trend of the symmetry energy, as depicted in solid curve, changes dramatically. In densities less than $\approx 4n_0$ it grows with density and its value is higher than that of the 2BF case, then after passing a maximum at $n_b \approx 0.7$ fm^{-3} it starts decreasing and its value becomes less than that of the 2BF prediction. Its

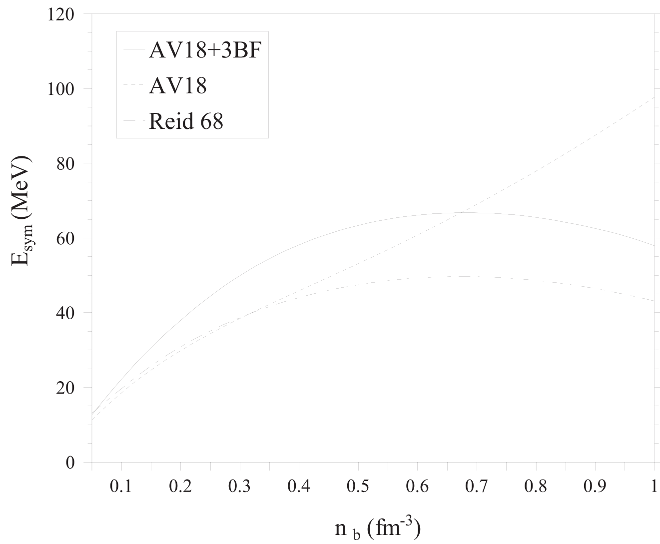

FIG. 1. Comparing nuclear symmetry energies predicted by the LOCV many-body method using different nuclear interactions.

value at saturation density is 31 MeV, which is in good agreement with experimental results and other theoretical methods. The qualitative behavior of the symmetry energy predicted by Reid 68 2BF (dash-dotted curve) is the same as that of the AV18 + UIX prediction (first ascending and then descending) though with smaller values. It gives $E_{\mathrm{sym}}(n_0) \approx 26$ MeV.

By determining the symmetry energy as a function of density, in Fig. 2 we present $\delta\mu$ as a function of proton fraction in $npe\mu$ matter. This result is due to a small compression that increases $n_b = 0.9$ fm^{-3} (dashed lines) to 1.0 fm^{-3} (solid lines). What seems interesting at first glance is the sign of the predicted $\delta\mu$'s. The arrows show the direction of the deviation from beta equilibrium (horizontal line) and so the sign of $\delta\mu$. AV18 + UIX and Reid 68, unlike AV18

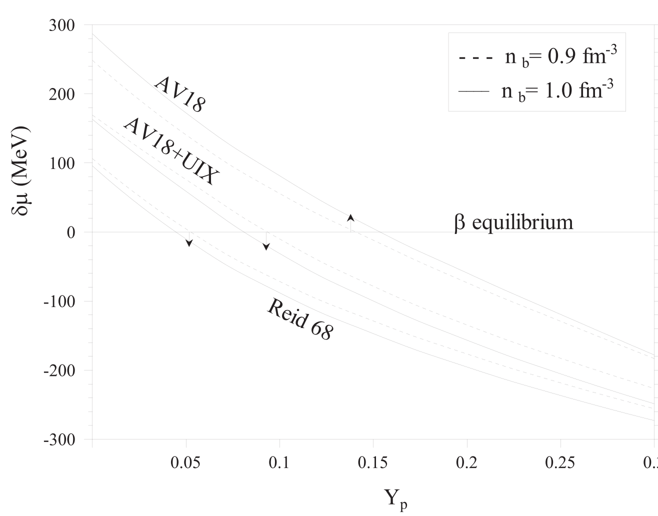

FIG. 2. Comparing $\delta\mu$ values, in an $npe\mu$ model of a NS, arising due to a small density change from 0.9 fm^{-3} (dashed lines) to 1.0 fm^{-3} (solid lines), predicted by the LOCV method supplemented by realistic interactions.

2BF, predict negative values for $\delta\mu$ in the considered density change. This, as was explained before, leads to the neutrino and antineutrino symmetry breaking in favor of neutrinos. These outcomes however, were expected from the behavior of the symmetry energies. In the case of purely ascending symmetry energies (like the prediction of AV18), as density grows, the beta equilibrium point shifts toward higher proton fractions (smaller isospin asymmetries) so the change in the density toward higher values makes the medium neutronized (hence $\delta\mu$ with a plus sign). The reverse process happens in the case of symmetry energies that have regions with descending behavior with respect to density (like the predictions of AV18 + UIX and Reid 68). In these regions, the density change toward higher values makes the medium protonized (hence $\delta\mu$ with a minus sign). Another important result depicted in Fig. 2 is the different prediction of absolute value of $\delta\mu$. It is around 9 MeV in the case of applying Reid 68, around 22 MeV (more than twice that of the Reid 68 prediction) in the case of using AV18, and 13 MeV when applying AV18 + UIX. These values, as seen in the next subsection, become much greater when hyperons are allowed to appear. Notice that these realistic values determine the nonthermal phase space for constructing the new beta equilibrium state. By comparing these values, even in the case of a small density change as we have adopted, with the order of magnitude of the thermal phase space ($\leqslant 0.1$ MeV), we find out that they are quite large. A point worth noticing that can influence the results is the precision of the calculations: since electrons are highly relativistic, a small change in their fraction can lead to dramatic changes in the $\delta\mu$ value. This is more obviously seen in the case of allowing hyperons to appear. We have adopted the calculation precision such that achieve the lower bound for the value of $\delta\mu$.

2. *Presence of free hyperons*

The presence of hyperons seems inevitable when the baryon density exceeds two times that of nuclear saturation [4] in many realistic EoSs. We have considered the influence of the presence of free Σ^- and Λ^0 on $\delta\mu$ to obtain a general view of this effect. In Fig. 3, we show $\delta\mu$ in the assumed typical density change (from $n_b = 0.9$ fm^{-3} to $n_b = 1.0$ fm^{-3}) and as a function of Y_p in the case of 2BFs only. The 3BF added case will be discussed separately. We find that the equilibrium Y_p in $n_b = 0.9$ fm^{-3}, while considered in the new density for calculating hyperons' and leptons' abundances, leads to Σ^- fraction greater than Y_p if we respect the common order of hyperon production, i.e., first Σ^- and then Λ^0. This is the case for most of the points with $Y_p < Y_p{}^{eq}$ (where $Y_p{}^{eq}$ refers to the final equilibrium asymmetry in the new density) and is clearly not consistent with the charge neutrality requirement. As was mentioned before, by allowing Λ^0 to appear first we are able to keep Y_{Σ^-} in the physical region. By applying this criteria for calculating $\delta\mu$, the first noticeable result seen in Fig. 3 is the increase in the value of $\delta\mu$ in both 2BF scenarios: $\approx$80 MeV in the case of the AV18 potential (around four times greater than that of one predicted by considering $npe\mu$ matter only) and $\approx$60 MeV in the case of the Reid 68 2BF interaction (more that six times larger). These dramatic changes in $\delta\mu$

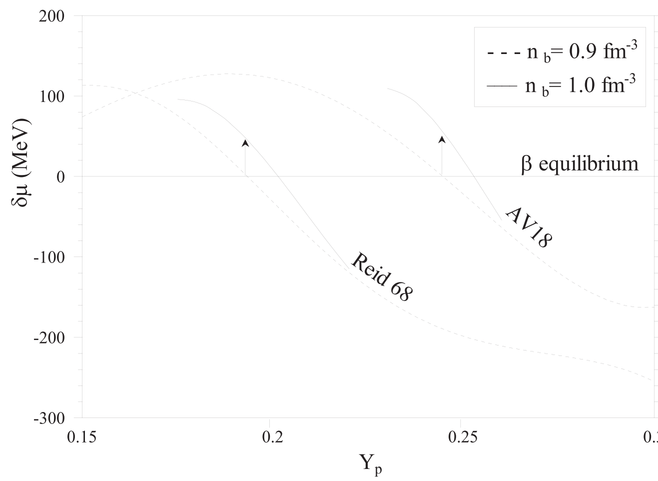

FIG. 3. The same as Fig. 2 but in the presence of free Σ^- and Λ^0 hyperons ($npe\mu Y$ model of a NS) and using only 2BF interactions.

value are due to the decrease of the relativistic electrons' fractions in favor of Σ^- production, which of course exceeds the decrease of nonrelativistic neutrons in favor of Λ^0's (see the diagrams of the composition of beta equilibrium matter in a neutron star with noninteracting hyperons using the LOCV method in Ref. [19]). As we noted in the previous section, these results are obtained in order to give the lower bound of $\delta\mu$. The more precise results are even larger. Another remarkable point is the change in the sign of $\delta\mu$ in the case of Reid 68 2BF, which is again a result of the significant decrease in the electron fraction.

By including 3BF effects in the case of the AV18 2BF interaction, $\delta\mu$, in the assumed density change, becomes ≈ -60 MeV. Here, the change in $\delta\mu$ value due to the presence of free hyperons is different from what occurred in the case of 2BFs only: it has become more negative. This is a consequence of more decrease in the neutron fraction than the electron fraction (Λ fraction exceeds that of Σ in the range of the typical density change [19] which is a direct result of more stiffness of the EoS due to the addition of the 3BF interaction). Here, in contrast with the case of 2BFs, more precise results are less negative (the absolute value becomes smaller). So, in our numerical procedure we have adopted the most accurate calculation possible for obtaining particle fractions and $\delta\mu$ in the case of AV18 + UIX.

B. Correlation factor

If the dUrca occurrence threshold is satisfied, the number spectra of neutrinos would dominantly be determined by neutrinos produced through this process. Otherwise, the neutron branch of mUrca is the more efficient process [3]. The previously mentioned threshold, $Y_p{}^{(\mathrm{dUrca})}$, in $npe\mu$ matter is slightly higher than that in npe matter. In Fig. 4, we show the beta equilibrium proton fractions in an $npe\mu$ model of the NS core predicted by the LOCV method implemented using AV18, AV18 + UIX and Reid 68 potentials in a baryon density range from 0.05 to 1.0 fm^{-3}. $Y_p{}^{(\mathrm{dUrca}\text{-}npe\mu)}$ is also presented. As is clearly seen, none of the strong interaction scenarios in

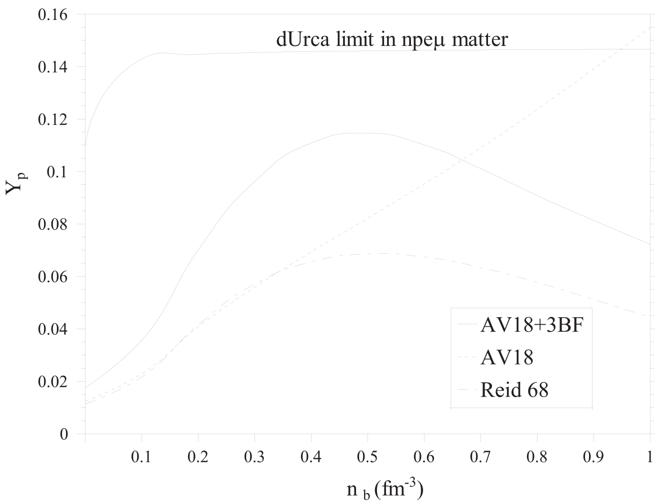

FIG. 4. Comparing beta equilibrium Y_p's in an $npe\mu$ model of a NS predicted by the LOCV method with realistic two- and three-body force interactions as input. The dUrca limit is also shown.

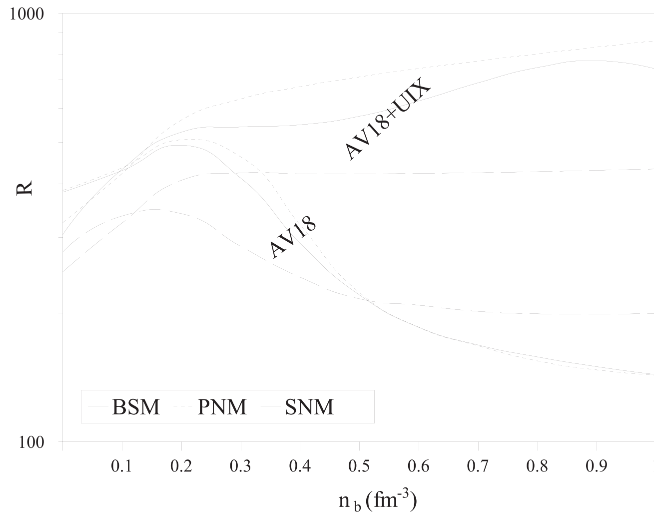

FIG. 5. Comparison of nuclear correlation factors [20] calculated with LOCV density-dependent correlation functions in three scenarios of the nuclear matter composition: pure neutron matter (PNM) with dotted curves, beta stable matter (BSM) with solid curves, and symmetric nuclear matter (SNM) with long dash curves, calculated using AV18 and AV18 + UIX interactions.

the adopted density range could satisfy the dUrca threshold except AV18 2BF (dotted curve). DUrca can be opened in this latter case in densities larger than $\approx 5.5n_0$. However, in this case too, mUrca would determine the number spectra of nonequilibrium neutrinos right after our typical density change happens (from 0.9 to 1.0 fm^{-3}). This is due to the fact that the equilibrium Y_p at $n_b = 0.9\ \mathrm{fm}^{-3}$ (0.14) does not satisfy the required condition of dUrca at $n_b = 1.0\ \mathrm{fm}^{-3}$. So, in what follows, we confidently concentrate on the number spectra of nonequilibrium electron neutrinos from the neutron branch of the mUrca process. This is also true for the case of considering hyperons. The presence of hyperons shifts the dUrca limit curve to even higher values by decreasing the electron fraction more than that of the neutron, especially in the case of the application of 2BFs. In the case of AV18 + UIX, in which, as was explained in the previous section, decreasing of the neutron fraction exceeds that of the electron, the dUrca limit may slightly shift to lower values at high densities. So, for this case, we have checked the dUrca condition at the assumed densities using the obtained particle fractions. It is not satisfied.

An important determining factor of the number spectra of nonequilibrium neutrinos produced in the n branch mUrca process, in relation (11), besides others, is the nuclear correlation factor $\mathcal{R}$. This parameter, completely calculated in Ref. [20], encapsulates the effect of nucleon correlations in the dense medium of the NS core through correlation functions extracted, in our work, directly from the LOCV many-body method. When the rapid change of the density occurs, the new correlation factor must be calculated in the final density with the proton fraction of the initial one, which refers to more or less asymmetric nuclear matter compared with the equilibrium asymmetry. In Fig. 5, we present the correlation factor calculated using LOCV density-dependent correlation functions in an $npe\mu$ model of the NS core. In this calculation we have applied three scenarios of composition of nuclear matter: beta-stable matter (BSM) with solid lines, symmetric nuclear matter (SNM) with dash-dotted curves, and pure neutron matter (PNM) with dotted lines. AV18 2BF and AV18 + UIX have been employed as strong interaction models. (We should emphasize that this figure is different from Fig. 5 in Ref. [20] in 3BF related curves. The 3BF-affected correlation functions applied there were obtained from a version of 3BF inclusion in LOCV that had errors. We overcame this deficiency in Ref. [28], using correct data from the modified extended version of LOCV [16], but $\mathcal{R}$ was reported for the BSM scenario only. In Fig. 5, we present $\mathcal{R}$ in all three scenarios with the correct data.) As seen, in AV18 case, in which the change of the density leads to a shift toward neutronization (PNM), this scenario and the equilibrium scenario predict almost the same values for the correlation factor in the whole density range considered. So, the correlation factor calculated in the non-equilibrium asymmetry can be replaced by the one calculated in the equilibrium state. In the case of AV18 + UIX, where at densities higher than $\approx 4n_0$ (Fig. 4) the change in the density leads to a shift toward protonization (SNM) (dash-dotted curve), the values of the equilibrium correlation factors and those out of equilibrium can be different. But, since the equilibrium proton fractions do not significantly differ, the difference in the correlation factors does not become remarkable either (e.g., less than 100 units deviation in a typical density change from $n_b = 0.5$ to 1.0 fm^{-3} in the case of AV18 + UIX). All these conclusions are also valid for the nucleonic sector of hypernuclear matter.

Before going to the next section, in which the overall impact of the relevant parameters on the number spectra of nonequilibrium neutrinos is displayed and discussed, we need to mention a point regarding the nucleon effective masses. In the framework of the LOCV method, the effective mass of nucleons has been calculated using single-particle potential energy at zero temperature only for symmetric nuclear matter

[29]. Fortunately, it has been shown in Ref. [30] that at zero temperature the defect functions arising from LOCV and BHF approaches are in good agreement, and the two methods, in similar conditions, give similar pair correlation functions for asymmetric nuclear matter. As a result, at $T = 0$ and for the same realistic nuclear interactions as in our LOCV calculation, we are allowed to employ BHF nucleon effective masses. These data are available for AV18 2BF and AV18 + UIX in Ref. [31] but not for the Reid 68 two-body interaction. In this latter case, we replace the nucleon effective masses with the bare ones. This is justified because, as shown in the next section, this nuclear matter description predicts very small values for the number spectra of nonequilibrium neutrinos compared with the other two descriptions, and employing the exact effective masses cannot significantly change the outcome. For the other two descriptions of the nuclear matter, i.e., AV18 and AV18 + UIX, by looking at Fig. 1 in Ref. [31] we see that at high densities the effective mass of neutrons for different proton fractions is almost the same. So we are allowed to use the equilibrium effective masses instead of those related to the exact nonequilibrium isospin asymmetry parameter. The same trend is also predicted for the effective mass of protons in the case of the AV18 scenario. In the case of the AV18 + UIX scenario however, a completely different behavior is seen: the values of the protons' effective mass for various proton fractions diverge as the baryon density increases. So for this case we would adopt the proton effective mass related to the exact nonequilibrium proton fraction. In the presence of hyperons, we employ the nucleon effective masses for the predicted nucleon density of the nucleonic subsystem and its related proton fraction (Y'_p).

C. Number spectra of nonequilibrium neutrinos

In Fig. 6 we have plotted the number spectra of nonequilibrium electron neutrinos or antineutrinos (the dominant one) in an $npe\mu$ model of a NS. The curves were obtained by assuming $T_9 = 1$ and using $\delta\mu$'s, $\mathcal{R}$ factors, particle fractions, and nucleon effective masses calculated in the proposed density change and within the previously explained nuclear descriptions. All values of the predicted number spectra were divided by the peak value of $\frac{d\Gamma}{dy}$ that belongs to the case of AV18 with the order of magnitude 10^{34} cm^{-3} s^{-1}. The order of magnitude of the particle fractions and correlation factors predicted by all three descriptions in the assumed condition is the same. Hence, the curves clearly show the important effect of the size of the nonthermal phase space suggested by each of them.

Figure 7 presents the same data as Fig. 6 but in the case of allowing the presence of free hyperons. As in the $npe\mu$ model, all values have been divided by the maximum value, that here has been obtained in the case of the AV18 + UIX description and is of the order 10^{37} cm^{-3} s^{-1}. Here, again, nuclear correlation factors have the same order of magnitude but the particle fractions do not. So in this model of a NS, the nonthermal phase space and the particle fractions are the competing factors in determining the number spectra of nonequilibrium neutrinos. We see that the nuclear description with larger $\delta\mu$ in our assumed density change (i.e., AV18 with $\delta\mu \approx 80$ MeV) predicts dramatically smaller values for the number of neutrinos than the description with smaller $\delta\mu$ (i.e., AV18 + UIX with $\delta\mu \approx 60$ MeV). This is due to the smaller electron fraction in the case of AV18, $O(10^{-4})$, compared with the corresponding value in the AV18 + UIX case, $O(10^{-3})$. Note that these electron abundances are calculated in the new density using the nonequilibrium proton fraction.

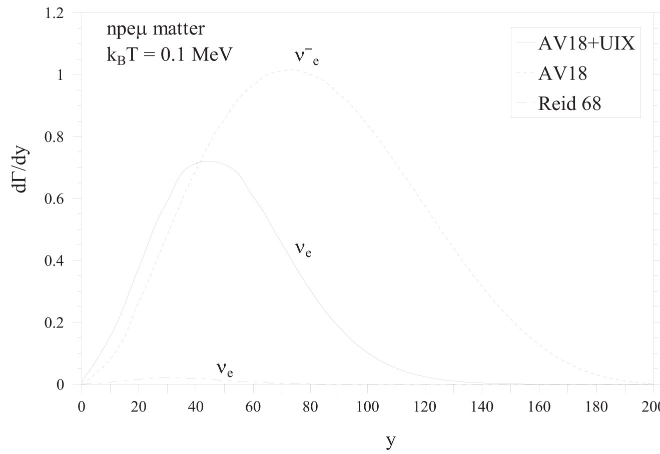

FIG. 6. Comparison of the number spectra of nonequilibrium neutrinos or antineutrinos (only the dominant flavors are presented) plotted with respect to the dimensionless parameter $y = \frac{E_\nu}{k_BT}$ in the density change from 0.9 to 1.0 fm^{-3} with $k_BT = 0.1$ MeV in the $npe\mu$ model of a NS predicted by the LOCV many-body method supplemented by different nuclear interactions. All values are normalized to the maximum value of $\frac{d\Gamma}{dy}$ that belongs to the case of AV18 and is of the order 10^{34} cm^{-3} s^{-1}.

V. DISCUSSION AND CONCLUSION

We calculated the number spectra of nonequilibrium electron neutrinos (or antineutrinos) produced in a cold NS core ($k_BT \leqslant 0.1$ MeV) undergoing a beta-equilibrium-disturbing

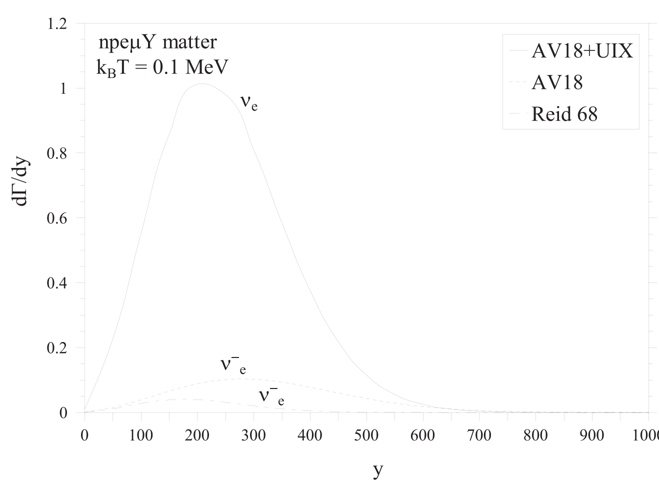

FIG. 7. The same as Fig. 6 but for the $npe\mu Y$ model of the NS core. Here the maximum value that all data are normalized to is of the order 10^{37} cm^{-3} s^{-1} and belongs to the case of AV18 + UIX.

astronomical process such as gravitational collapse into a black hole, radial pulsations, or spin-down that allows only $\delta\mu \ll \mu_i$. We investigated the effect of applying a realistic description of the strong interaction in the superdense matter of NSs on this quantity. For this purpose, we focused on a small compression and a typical density change from 0.9 to 1.0 fm^{-3} at the initial instance of the occurrence of the relevant process. We calculated the main input of this quantity, i.e., the nonthermal phase space opened by beta equilibrium breaking ($\delta\mu$), in an $npe\mu$ and a hypernuclear (including free Σ^-'s and Λ^0's) model of the NS core described by a variational many-body method (LOCV) and realistic 2BFs (AV18 and Reid 68). We also considered the effect of 3BF inclusion through a UIX model in the case of the AV18 interaction using the modified extended version of LOCV (AV18 + UIX). As explained in detail in the Results section, all these nuclear descriptions based on their different predictions of the density dependence of the symmetry energy suggest different values and signs for $\delta\mu$. By examining the impact of the presence of free hyperons on $\delta\mu$, we realized that it has a noticeable influence on the size of the nonthermal phase space and its overall effect is to predict larger values for the number spectra of nonequilibrium neutrinos. In the absence of the dUrca process, when the n branch of mUrca is the dominant mechanism of neutrino production, we studied the effect of the nonequilibrium processes on the nuclear correlation factor as another input parameter. It was shown that this parameter can be replaced by its corresponding value calculated in the equilibrium asymmetry of the final density. Nonequilibrium particle fractions were also seen to have a determining influence on the final result.

To provide a comparison with other investigations, we calculated $\delta\mu$ predicted by the EoSs suggested in a work by Prakash *et al.* [11] and applied by Ref. [10] to obtain an upper bound for the neutrino burst accompanying the NS gravitational collapse to a black hole. Using three EoSs in Ref. [11] with different choices of the potential contribution to the symmetry energy [$F_1(u) = u,\ F_2(u) = \frac{2u}{1+u^2},\ F_3(u) = \sqrt{u}$, where $u = \frac{n_b}{n_0}$] and with their parameters adjusted to the saturation incompressibility of SNM (i.e., at $n_b = n_0$), $K_0 = 180$ MeV(referring to them as PAL1, PAL2, and PAL3 respectively as in Ref. [10]), we saw that in the case of $npe\mu$ matter the predicted $\delta\mu$ values in the density change from 0.9 to 1.0 fm^{-3} were almost the same as what we obtained with our realistic descriptions: $\delta\mu^{(\mathrm{PAL1})} \approx 20$ MeV, $\delta\mu^{(\mathrm{PAL2})} \approx 24$ MeV, $\delta\mu^{(\mathrm{PAL3})} \approx 7$ MeV. However, since the trend of the density dependence of the symmetry energy predicted by these EoSs is purely ascending with respect to baryon density, they all give positive $\delta\mu$. Also, they all satisfy the dUrca condition. So, their prediction for the neutrino burst, especially in the case of PAL2, is in fact the upper bound. As we showed, considering the presence of hyperons in the NS medium has a great bearing on the nonthermal phase space, but this was not accounted for in Ref. [10]. We calculated $\delta\mu$ in the presence of free Σ^- and Λ^0 for these three EoSs and found that it did not change sensitively. This is because these EoSs correspond to $K_0 = 180$ MeV and they are not stiff enough to allow for Λ production below $n_b = 1.0$ fm^{-3}. Also, Σ^- production happens just before or at $n_b = 0.9$ fm^{-3}. So here, for the density change considered, hyperon appearance does not affect the $\delta\mu$ value noticeably compared with the $npe\mu$ case. However, due to the dUrca process, the predicted number spectrum of nonequilibrium neutrinos is much greater than those obtained by our realistic results in the cases of PAL1 and PAL2 EoSs. We think that if the presence of hyperons in stiffer versions of the mentioned nuclear EoSs is considered, the estimated neutrino burst in Ref. [10] might shift to higher values that are detectable from Earth. Such a detection with a dominant flavour can potentially provide a diagnostic for the properties of the available EoSs at high densities. In general, we conclude that considering the effect of other degrees of freedom in studying nonequilibrium phenomena leads to very different results and so seems essential.

ACKNOWLEDGMENTS

This work was partially supported by the Iran National Science Foundation (INSF) under Grant No. 97024312.

APPENDIX A: VALIDITY OF NON-ADIABATIC DENSITY CHANGE

It is obvious that all our investigations and achievements in the present study depend on whether or not our realistic descriptions of the NS medium result in a timescale for beta relaxation that is large enough compared with the typical timescale of the density change in related phenomena. Here, by presenting an estimation of the relaxation time we show that our applied realistic descriptions of the NS matter do really satisfy the required condition. Recall that we work in the high degeneracy regime ($k_BT \leqslant 0.1$ and $\delta\mu \ll \mu_i$), i.e., where the thermal and nonthermal phase spaces needed for weak reactions to proceed and construct the new equilibrium are very limited. Calculation of the relaxation time (τ_{relax}, referred to as τ_β in the context of our paper) is presented in [3] (hereafter referred to as paper I). In paper I, the relaxation time is estimated when the dimensionless measure of the departure from beta equilibrium is very small ($\xi \ll \frac{\delta\mu}{k_BT}$). The results when nucleon direct (d) and modified (m) Urca processes are responsible for establishing the new equilibrium state are $\tau^{(d)}_{\mathrm{relax}} \approx 20T_9^{-4}$ s and $\tau^{(m)}_{\mathrm{relax}} \approx T_9^{-6}$ months, respectively, where as before $T_9 = T/10^9$ K. So, in a not too hot NS where the high degeneracy condition is satisfied and the departure from beta equilibrium is not too large, the relaxation toward equilibrium is very slow. In the condition of $\xi \gg 1$, however, which is the prediction of our realistic descriptions, we deal with larger nonthermal phase space arising from beta equilibrium violation. Qualitatively speaking, this increase in the size of the nonthermal phase space naturally accelerates the beta processes and this acceleration ceases the increase of τ_{relax} due to the larger deviation from equilibrium. The increase of τ_{relax} becomes very slow or even stops but the slowness of weak interactions compared with the timescale of density change in the relevant phenomena ($\approx$ milliseconds or less) is still valid. In order to quantitatively show the correctness of this general argument in the case of our realistic descriptions of the NS medium, we estimate τ_{relax} for the condition described in our study: a sudden increase in the density that changes $n_b = 0.9\ \mathrm{fm}^{-3}$ to $n_b = 1.0\ \mathrm{fm}^{-3}$. It was seen in Sec. IV that, within our nuclear descriptions and the typical density change, the modified Urca process is responsible for constructing the new beta equilibrium. So, we present an estimation of τ_{relax} for this process. As in paper I, we start from $\delta\dot{\xi} = (\partial\delta\mu/\partial Y_p)\dot{Y}_p/(k_B T) = \chi\Delta\Gamma/(k_B T)$, where $\chi = -(\partial\delta\mu/\partial Y_p)/n_b$ and $\Gamma = \Gamma_{n\to p} - \Gamma_{p\to n} = n_b\dot{Y}_p$. Using our obtained $\frac{d\Gamma^{(m)}}{dy}$ in Eq. (11) and the $\delta\mu$ expression in Eq. (15), and doing the integration that gives $\Delta\Gamma$, we reach the following relation for $\frac{d\xi}{dt}$:

$$\begin{aligned}\dot{\xi} &= \left[2.64\times10^{-12}\frac{E_{\mathrm{sym}}}{n_b} + 6.42\times10^{-10}(n_bY_p)^{-2/3}\frac{\partial Y_e}{\partial Y_p}\right]\\ &\quad\times\frac{Y_e^{2/3}Y_p^{1/3}}{Y_n^2}\frac{n_0}{n_b}\left(\frac{m_n^*}{m_n}\right)^3\left(\frac{m_p^*}{m_p}\right)\mathcal{R}\,T_9^6\,\xi\,H(\xi)\\ &= \kappa\,T_9^6\,\xi\,H(\xi),\end{aligned} \tag{A1}$$

where $H(\xi) = 1 + \frac{189\xi^2}{367\pi^2} + \frac{21\xi^4}{367\pi^4} + \frac{3\xi^6}{1835\pi^6}$.

As is apparent from Figs. 1, 4, and 5, the following orders of magnitude for the input parameters of relation (24) are predicted within our realistic descriptions: $Y_i \approx O(0.1)$, $0.5 \leqslant \frac{\partial Y_e}{\partial Y_p} \leqslant 1$ in the $npe\mu$ model of the NS core, $E_{\mathrm{sym}} \approx O(10^2)$, $\mathcal{R} \approx O(10^2\text{–}10^3)$, and $\frac{m^*}{m} \approx O(0.1\text{–}1)$. We assume that $T_9 = 1$ ($k_BT = 0.1$ MeV). For $\xi \ll 1$, e.g., $\xi = 0.1$, we have $H \approx 1$ and the integration for obtaining τ_{relax} can be done analytically. The limits of the integration are set as $\xi = 0.1$ to $\xi = 0.1/e$ where e is Napier's constant. Applying the mentioned orders of magnitude of the parameters, we get $\tau_{\mathrm{relax}} = \frac{1}{\kappa}T_9^{-6} \approx 175$ days. For $\xi \gg 1$, e.g., $\xi = 10$ however, the integration for estimating τ_{relax} must be done numerically. We set the lower and upper bounds of the integration as $\xi = 10$ and $\xi = 0.1/e$ respectively. The upper bound is set in correspondence with the upper bound of the case $\xi \ll 1$ to make the comparison possible. This time, we obtain $\tau_{\mathrm{relax}} = 4.5\frac{1}{\kappa}T_9^{-6} \approx 780$ days. However, for $\xi \approx O(10^2)$, predicted in our work for the $npe\mu$ model, we see that $H(\xi)$ and so τ_{relax} remain almost the same and no longer increase, but anyway τ_{relax} is very large compared with the timescale of the change of the density. For $\xi > O(10^2)$, that occurs in the case of the appearance of free hyperons, H does not change sensitively and other input parameters are almost in the same range as for nuclear matter. So, allowing free hyperons to appear does not change the obtained outcome either.

APPENDIX B: BRIEF DESCRIPTION OF LOCV METHOD

The LOCV method is a microscopic and self-consistent many-body framework for calculating the bulk properties of nuclear matter. The many-body energy E is calculated from the expectation value of our Hamiltonian in the form

$$\hat{\mathcal{H}} = \sum_i \frac{\hat{p}_i^2}{2m_i} + \sum_{i<j}\hat{V}_{ij} + \sum_{i<j<k}\hat{V}_{ijk} + \cdots. \tag{B1}$$

where $\hat{V}_{ij}$ ($\hat{V}_{ijk}$) is the realistic two-body (three-body) potential. The expectation value of energy is written in the following form using cluster expansion:

$$E(A) = \frac{1}{A}\frac{\langle\Psi|\hat{\mathcal{H}}|\Psi\rangle}{\langle\Psi|\Psi\rangle} = E_1 + E_2 + \cdots, \tag{B2}$$

where A is the total number of nucleons. The trial wave function Ψ of the interacting system is considered as

$$\Psi(12\ldots A) = \hat{\mathcal{F}}(12\ldots A)\Phi(12\ldots A), \tag{B3}$$

where Φ is the uncorrelated Fermi system wave function and $\hat{\mathcal{F}}$ is the many-body correlation function considered as an operator. This correlation operator is taken as the symmetric product of pair correlation operators $[\hat{f}(ij)]$ in Jastrow form [32], i.e.,

$$\hat{\mathcal{F}}(12\ldots A) = \hat{\mathcal{S}}\prod_{i<j}\hat{f}(ij), \tag{B4}$$

where $\hat{\mathcal{S}}$ is the symmetrizing operator. The one-body energy E_1 in Eq. (25) is the familiar Fermi gas kinetic energy of the A-body system. The two-body energy is defined as

$$E_2 = \frac{1}{2A}\sum_i \langle ij|\hat{\mathcal{W}}(12)|ij\rangle_a, \tag{B5}$$

where $\hat{\mathcal{W}}(12)$ is an effective two-body potential defined by

$$\hat{\mathcal{W}}(12) = [f(12), [\hat{T}_1 + \hat{T}_2, \hat{f}(12)]] + \hat{f}(12)\hat{V}\hat{f}(12), \tag{B6}$$

in which $\hat{T}_1 + \hat{T}_2$ is the kinetic energy operator of a non-interacting (1,2) pair and $\hat{V}(1,2)$ is the interparticle potential operator. We can write the two-body energy as a functional of correlation functions:

$$E_2[f] = \int \mathfrak{L}(f', f, r)dr, \tag{B7}$$

where $\mathfrak{L}$ depends on correlation functions f and their radial derivatives, and N-N potential parameters act as an input. The expression of two-body energy can now be minimized with respect to the channel correlation functions, but subject to the normalization constraint which is considered in the LOCV method by [15]

$$\frac{1}{A}\langle ij|f_{\mathrm{pc}}^2(12) - f_k^2(12)|ij\rangle_a = 1. \tag{B8}$$

The function f_{pc} is the modified Pauli correlation function which for SNM at zero temperature has the form

$$f_{\mathrm{pc}} = \left(1 - \frac{9}{4}\left(\frac{j_1(r_{12})}{r_{12}}\right)^2\right)^{-1/2}, \tag{B9}$$

where $j_1(r_{12})$ is the spherical Bessel function of order 1. This constraint introduces a Lagrange multiplier through which all f's are coupled. So we end up with a set of Euler-Lagrange equations for correlation functions subject to the normalization constraint. It is noticeable that $\chi = \langle\psi_{12}|\psi_{12}\rangle - 1$ has the role of a smallness parameter in the cluster expansion and by choosing an appropriate correlation function we can truncate the expression (28) up to two-body terms and keep the higher terms as small as possible [33]. Finally, the correlation functions are extracted by solving the arising coupled differential equations. More details can be found in Ref. [34] and the references therein.

It is well known that two-body forces alone cannot reproduce the saturation properties of symmetric nuclear matter. Also the three-body forces play an important role at supernormal densities of nuclear systems [35]. The three-body forces are successfully included in LOCV method which reproduces the correct bulk properties of nuclear matter at the saturation point. To avoid the full three-body problem, the three-body interaction (semiphenomenological UIX interaction) is included via an effective two-body potential derived after averaging out the third particle, which is weighted by the LOCV two-body correlation functions $f_k(ij)$ at a given number density n_N. For more details, refer to Ref. [16].

---

[1] D. G. Yakovlev and C. J. Pethick, Annu. Rev. Astron. Astrophys. **42**, 169 (2004).
[2] J. N. Bahcall and R. A. Wolf, Phys. Rev. **140**, B1452 (1965).
[3] D. G. Yakovlev, A. D. Kaminker, O. Y. Gnedin, and P. Haensel, Phys. Rep. **354**, 1 (2001).
[4] V. A. Ambartsumyan and G. S. Sakyaan, Astron. Zh. **37**, 193 (1960).
[5] C. J. Hansen, Nature (London) **211**, 1069 (1966).
[6] C. J. Hansen and S. Tsuruta, Can. J. Phys. **45**, 2823 (1967).
[7] A. Finzi and R. A. Wolf, Astrophys. J. **153**, 835 (1968)
[8] M. E. Gusakov, D. G. Yakovlev, and O. Y. Gnedin, Mon. Not. R. Astron. Soc. **361**, 1415 (2005).
[9] W. D. Langer and A. G. W. Cameron, Astrophys. Space Sci. **5**, 213 (1969).
[10] E. Gourgoulhon and P. Haensel, Astron. Astrophys. **271**, 187 (1993).
[11] M. Prakash, T. L. Ainsworth, and J. M. Lattimer, Phys. Rev. Lett. **61**, 2518 (1988).
[12] A. Reisenegger, Astrophys. J. **442**, 749 (1995).
[13] J. C. Owen, R. F. Bishop, and J. M. Irvine, Nucl. Phys. A **177**, 45 (1776).
[14] J. C. Owen, R. F. Bishop, and J. M. Irvine, Ann. Phys. (NY) **102**, 170 (1976).
[15] M. Modarres and J. M. Irvine, J. Phys. G **5**, 511 (1979).
[16] S. Goudarzi and H. R. Moshfegh, Phys. Rev. C **91**, 054320 (2015); **96**, 049902(E) (2017).
[17] R. B. Wiringa, V. G. J. Stoks, and R. Schiavilla, Phys. Rev. C **51**, 38 (1995).
[18] R. V. Reid, Jr., Ann. Phys. (NY) **50**, 411 (1968).
[19] M. Shahrbaf, H. R. Moshfegh, and M. Modarres, Phys. Rev. C **100**, 044314 (2019).
[20] A. Dehghan Niri, H. R. Moshfegh, and P. Haensel, Phys. Rev. C **93**, 045806 (2016).
[21] P. Haensel, Astron. Astrophys. **262**, 131 (1992).
[22] D. Pines and P. Noziéres, *The Theory of Quantum Liquids* (Benjamin, New York, 1966), Vol. I.
[23] S. L. Shapiro and S. A. Teukolsky, *Black Holes, White Dwarfs, and Neutron Stars* (Wiley Interscience, New York, 1983).
[24] R. F. Sawyer and A. Soni, Astrophys. J. **230**, 859 (1979).
[25] P. Haensel and A. J. Jerzak, Astron. Astrophys. **179**, 127 (1987).
[26] I. E. Lagaris and V. R. Pandharipande, Nucl. Phys. A **369**, 470 (1981).
[27] I. Bombaci and U. Lombardo, Phys. Rev. C **44**, 1892 (1991).
[28] A. Dehghan Niri, H. R. Moshfegh, and P. Haensel, Phys. Rev. C **98**, 025803 (2018).
[29] M. Modarres and A. Rajabi, Nucl. Phys. A **867**, 1 (2011).
[30] M. Baldo and H. R. Moshfegh, Phys. Rev. C **86**, 024306 (2012).
[31] M. Baldo, G. F. Burgio, H. J. Schulze, and G. Taranto, Phys. Rev. C **89**, 048801 (2014).
[32] R. Jastrow, Phys. Rev. **98**, 1479 (1955).
[33] H. R. Moshfegh and M. Modarres, J. Phys. G: Nucl. Part. Phys. **24**, 821 (1998).
[34] M. Modarres and M. Moshfegh, Prog. Theor. Phys. **112**, 21 (2004).
[35] B. S. Pudliner, V. R. Pandharipande, J. Carlson and R. B. Wiringa, Phys. Rev. Lett. **74**, 4396 (1995); B. S. Pudliner, V. R. Pandharipande, J. Carlson, S. C. Pieper, and R. B. Wiringa, Phys. Rev. C **56**, 1720 (1997).